# Chapter 1

# Introduction of the sphere map with application to spin-torque nano-oscillators

Keith Gilmore[1] and Robert Gilmore[2]

aindx]Gilmore, Keith and Gilmore, Robert

[1] *The Molecular Foundry*
*Lawrence Berkeley National Laboratory*
*Berkeley, CA 94720*
*USA*

[2] *Physics Department*
*Drexel University*
*Philadelphia, PA 19104*
*USA*

## Contents

1. Introduction of the sphere map with application to spin-torque nano-oscillators 1

*Keith Gilmore[1] and Robert Gilmore[2]*
We generalize the circle map $S^1 \to S^1$ to a nonlinear mapping of the sphere to itself. The sphere map $S^2 \to S^2$ depends on the three parameters that describe the rotation operations in the group $SO(3)$ and one nonlinear parameter that describes the strength of a folding acting on the sphere surface. This new map is used to study the properties of a spin valve that obeys equations of the form $\dot{X}_i = -b_{ij}X_j + c_{ijk}X_jX_k$ and satisfy the conservation condition $\frac{d}{dt}\sum X_i^2 = 0$. With periodic driving, we find regions in the parameter space that describe quasiperiodic, mode-locked, and chaotic behavior.

## 1. Introduction

In this work we formulate tools to study the spectrum of possible behaviors of a magnetic nano-oscillator that is described by the Landau-Lifshitz-Slonczewski (LLS) equations. These equations have a form introduced by Lorenz in his study of truncations of the Navier-Stokes equations.

Within the LLS equations, the magnetization is a conserved quantity, so is described by a point on the surface of a sphere $S^2$. Under periodic forcing the phase space is enlarged to $S^2 \times S^1$. We introduce a mapping of the sphere surface to itself, which is a generalization of the circle map, to study the dynamics of this system.

In Sect. 2 we review the circle map, as defined by Kolmogorov and Arnold. We also review the truncated form of the Navier-Stokes equations, as described by

Lorenz. Sect. 3 discusses spin-transfer-torque and introduces the Landau-Lifshitz-Slonczewski equations. In Sect. 4 we bring the LLS equations into the form proposed by Lorenz. Sect. 5 defines the sphere map $S^2 \to S^2$. In Sect. 6 we introduce three large-scale scans for behavior under rotations about three coordinate axis. Sect. 7 examines some appropriate bifurcation diagrams, and in Sect. 8 we investigate how some trajectories behave under variation of the nonlinear coupling strength. Finally, we summarize our findings in Sect. 9.

## 2. Background

The circle map

$$\theta_{n+1} = \omega_0 + \theta_n - k\sin(\theta_n) \tag{1}$$

was originally introduced by Kolmogorov to describe the behavior of periodically driven mechanical oscillators.[1] Here $\theta$ represents the phase of the oscillator and $\theta_n$ is its value stroboscopically recorded (i.e., at the same phase during each driving period). The term $-k\sin(\theta_n)$ describes the nonlinearity in the response of the oscillator to the driving force. Arnold later used this map to study the breakup of invariant tori under perturbations.[2] The circle map exhibits behavior including quasiperiodic orbits (regular but not closed), mode locked regions, Arnold tongues, and period-doubling routes to chaotic behavior.[3]

A standard way to simplify the Navier-Stokes equations involves expanding the various fields present (the velocity, temperature, and pressure fields) in Fourier modes or empirical orthogonal modes, placing these representations in the Navier-Stokes equations, and then integrating out the spatial dependence. Lorenz[4] noted that the resulting set of ordinary differential equations for the time-dependent mode amplitudes assumes the form of a set of ordinary differential equations whose source terms are polynomials of degree no greater than two:

$$\frac{dX_i}{dt} = a_i - b_{ij}X_j + c_{ijk}X_jX_k \tag{2}$$

where the tensor $c$ is symmetric in the last two indices: $c_{ijk} = c_{ikj}$ and we use the summation convention. Lorenz further observed that all initial conditions lead to bounded solutions if $b_{ij}$ is positive definite and the quadratic terms satisfy the condition $c_{ijk}X_iX_jX_k = 0$. These conditions are satisfied by the Lorenz equations.

The Lorenz equations exhibit a behavior that was very surprising for its time: deterministic but nonperiodic flow.[4] The Lorenz strange attractor has been a model for understanding chaotic behavior and a test-case for tools developed to study this behavior.[5]

Spintronics, the control of magnetic systems with spin-currents, holds great technological promise. Some of the interactions of spin-currents with magnetic systems are described by the Landau-Lifshitz-Slonczewski equations. These equations have the form of Eq.(2) with $a_i = 0$, $b_{ij}$ antisymmtric and $c_{ijk}$ with mixed symmetry

and $c_{ijk}X_iX_jX_k = 0$. As a result, the phase space for the magnetic moment is the sphere surface $S^2$. The LLS equations for a periodically driven system involve flows on a three-dimensional phase $S^2 \times S^1$. Since the phase space is three-dimensional, chaotic behavior is possible.[3] A Poincaré section can be chosen as $\phi = \text{cst.}, \phi \in S^1$. The Poincaré first return map is the map $S^2 \to S^2$. The sphere map is a generalization of the circle map. We report some of the properties of the sphere map in this work.

## 3. Landau-Lifshitz-Slonczewski Equations

Ferromagnetism is a state of matter in which strong Coulomb exchange interactions align the spins of electrons, producing a net magnetization in the absence of any applied external field. The exchange interaction is short range. On longer length scales the magnetostatic dipole interaction favors antiparallel alignment of spins, leading to the formation of magnetic domains. The electron spins within a given domain are essentially uniformly aligned. Neighboring domains are typically oriented so as to minimize the magnetostatic dipole energy. Between two domains the magnetization rotates smoothly from one domain orientation to the orientation of the neighboring domain producing a magnetic domain wall. The characteristic length scale of domains depends on material parameters and sample geometry, but is large enough for many materials, such as the transition metals, that nanoscale samples can be comprised of a single domain and thought of as having one macroscopic magnetic moment.

It is energetically favorable for the magnetization to align with the effective magnetic field, which consists of the combination of internal and external fields. Because the magnetization carries angular momentum, the effective field applies a torque to the magnetization, which causes the magnetization to precess about the effective field according to

$$\partial_t \hat{\mathrm{m}} = -\gamma \hat{\mathrm{m}} \times \mathbf{H}^{\mathrm{eff}} \tag{3}$$

where $\hat{\mathrm{m}}$ is a unit vector designating the direction of the magnetization, $\mathbf{H}^{\mathrm{eff}}$ is the effective magnetic field, and $\gamma$ is the gyromagnetic ratio. If $\mathbf{H}^{\mathrm{eff}}$ is constant in time then $|\gamma \mathbf{H}^{\mathrm{eff}}|$ is the precession frequency.

In reality, some loss mechanism damps the precession of the magnetization, causing it to align in the low energy direction specified by the effective field. This damping is a phenomenological observation that is typically accounted for by the inclusion of another torque, $-(\lambda/|\mathrm{m}|)\,\hat{\mathrm{m}} \times \left[\hat{\mathrm{m}} \times \mathbf{H}^{\mathrm{eff}}\right]$, that is orthogonal to both the magnetization direction and the precession direction. Together, these two torques form the Landau-Lifshitz (LL) equation[6]

$$\partial_t \hat{\mathrm{m}} = -\gamma \hat{\mathrm{m}} \times \mathbf{H}^{\mathrm{eff}} - \frac{\lambda}{|\mathrm{m}|} \times \hat{\mathrm{m}} \times \mathbf{H}^{\mathrm{eff}}\,. \tag{4}$$

The parameter $\lambda$ is a sample dependent dissipation rate. The damping term is often

rewritten in the equivalent Gilbert form[7–9] as $\alpha\hat{\mathrm{m}} \times \partial_t \hat{\mathrm{m}}$ and the resulting equation referred to as the Landau-Lifshitz-Gilbert equation (LLG equation). In the present work we use the Landau-Lifshitz form.

The magnetization of a material may also be manipulated by an electrical current.[10–13] Due to the inequivalent density of states of each spin type at the Fermi level, a current flowing through a magnetic material will be spin-polarized – it will carry angular momentum in addition to charge. If the magnetization direction of a material is spatially non-uniform along the direction of current flow the spin-polarized current will apply a torque to the magnetization. This torque is known as the spin-transfer torque. The spin-transfer torque shows promise for use in magnetic random access memories[14,15] and telecommunication applications.[16,17]

The spin-transfer torque can have different forms depending on the physical circumstances under consideration.[18] If the magnetization changes very slowly in space, such as in a wide domain wall, then the spin-orientation of the transport electrons will be able to track the local magnetization adiabatically as the electrons flow through the system. In this case, the torque due to the spin current is referred to as the adiabatic spin torque.[10] If the spatial variation of the magnetization is abrupt, the spin orientation of the transport electrons will not be able to respond adiabatically to the local magnetization and the resulting torque is the non-adiabatic spin torque.[13] In this paper we will consider the non-adiabatic spin torque such as occurs in a nano-pillar magnetic multilayer.

The nano-pillar magnetic multilayer system consists of a multilayer nano-pillar connected on both ends to non-magnetic electrodes. The multilayer stack has a physical cross-section of a few tens of nanometers and two (or more) magnetic layers separated by non-magnetic spacer layers. The magnetization of one of the magnetic layers will be fixed (either through exchange biasing or simply by being much thicker than the second magnetic layer); this is referred to as the fixed layer or polarizer. The magnetization of the other magnetic layer will be free to rotate; this layer is referred to as the free layer.

As a current flows through the multilayer stack it becomes spin-polarized by the polarizer layer. The spin-polarized current then impinges upon the free layer, applying a non-adiabatic spin-torque, $\Omega\hat{\mathrm{m}} \times [\hat{\mathrm{m}} \times \hat{\mathrm{m}}_{\mathrm{P}}]$, to the magnetization. The prefactor $\Omega$ is a constant with dimensions of frequency that depends on the current density, material parameters, and fundamental constants. The unit vector $\hat{\mathrm{m}}_{\mathrm{P}}$ is the direction of magnetization of the fixed layer, which dictates the polarization axis for the spin current. Adding this spin-torque to the LL equation gives gives the Landau-Lifshitz-Slonczewski (LLS) equation

$$\partial_t \hat{\mathrm{m}} = -\gamma \hat{\mathrm{m}} \times \mathbf{H}^{\mathrm{eff}} - \frac{\lambda}{|\mathrm{m}|} \hat{\mathrm{m}} \times \hat{\mathrm{m}} \times \mathbf{H}^{\mathrm{eff}} + \Omega \hat{\mathrm{m}} \times \hat{\mathrm{m}} \times \hat{\mathrm{m}}_{\mathrm{P}} \,. \tag{5}$$

All three torques in this equation are perpendicular to the magnetization and act only to rotate the magnetization, not change its magnitude. Therefore, the trajectory of $\mathbf{m}(t)$ evolves on the surface of a sphere $S^2$. Since the sphere is two-

dimensional the asymptotic behavior can only be stationary or periodic, corresponding to the the only behaviors allowed by the Poincaré-Bendixon theorem.[3]

The dynamic responses allowed by Eq. (5) have been studied both experimentally[19] and theoretically.[20] Three types of behavior are observed. Either the magnetization of the free layer will remain largely unperturbed, will reverse, or will be driven into a stable precession orbit. The particular response depends on the current density, degree of polarization, strength and direction of external and internal fields, and the strength of the damping. For low spin-current driving, the damping torque keeps the magnetization oriented in the low energy direction. Very large spin-currents will cause the direction of the magnetization of the free layer to reverse and align in the oppositely oriented low energy direction. Intermediate spin-current driving can establish stable precession orbits. The frequency of these precession orbits may be tuned by adjusting the current density. This observation suggests an application for the spin-torque multi-layer as a voltage-controlled tunable-frequency oscillator.[16,17] These observations assume a dc-current. In this work we investigate what dynamic responses may be induced by an ac-current.

## 4. Connection with Lorenz Equations

The Landau-Lifshitz-Slonczewski equations (4) have the form of the Lorenz equations (2) under the identification $m_1 = X_1 = X$, $m_2 = X_2 = Y$, and $m_3 = X_3 = Z$. In this form $a_i = 0$, $b_{ij} = -b_{ji}$, and $c_{ijk}$ is of mixed symmetry with $c_{ijk}X_iX_jX_k = 0$.[4]

If any one of the terms in Eq.(4) is periodically driven, the phase space is enlarged to $S^2 \times S^1$. This occurs in the same way and for the same reasons that the phase space for nonlinear two-dimensional oscillators (e.g., $R^2$ for the Duffing and van der Pol oscillators) is enlarged to $R^2 \times S^1$ when they are periodically driven.[21,22] In this three-dimensional phase space more exciting behaviors can occur.[3] These include quasiperiodic behavior, periodic behavior due to mode locking, and chaotic behavior. All these types of behavior have been seen in simulations[23–25] and discussed in a recent review article.[26] At the present time there is no systematic understanding of the parameter ranges under which these three types of behavior can be exhibited by the solutions of the periodically driven LLS equations or the nano-oscillators that they model. It would be extremely useful to have a systematic understanding, comparable to that provided by the circle map, for a large class of nonlinear dynamical systems. The purpose of the present contribution is to provided the tools for such a systematic understanding of the parameter space describing the behavior of the solutions of Eq.(5).

Since the phase space is $S^2 \times S^1$, it is useful to study dynamics by studying the first return map on the Poincaré section. The Poincaré section can be chosen as a stroboscopic section $2\pi t/T = \text{cst. mod } 2\pi$. This is a sphere. We call the first return map $S^2 \to S^2$ the *sphere map* in analogy with maps $S^1 \to S^1$, the widely studied

circle maps.[1–3] These maps have been enormously useful for the study of nonlinear oscillators in the plane that have undergone a Hopf bifurcation and are periodically driven (e.g., van der Pol oscillator). We expect sphere maps to be equally useful for studying the properties of nonlinear spherical oscillators such as spin valves.

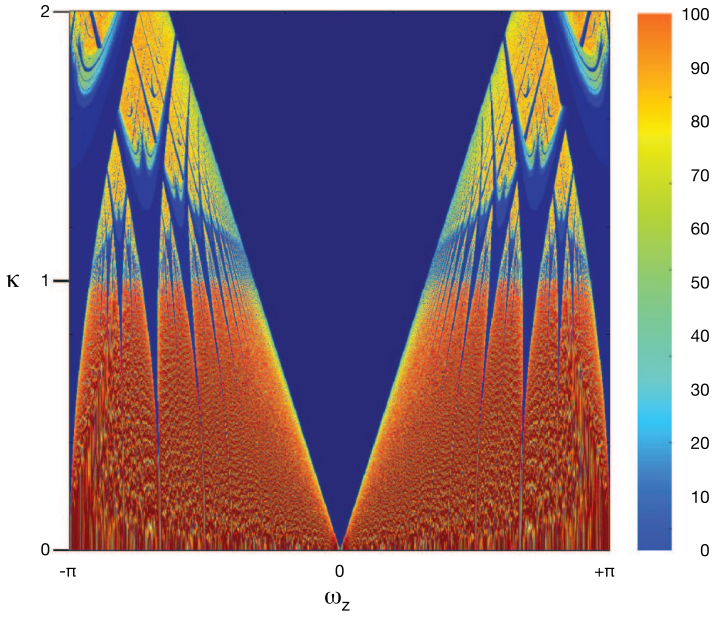


Fig. 1. (color online) Behavior of the sphere map for rotations about the $z$-axis $(0, 0, 1)$. Color coding: number of distinct points in a long trajectory. Cool colors (blues) indicate low period orbits that exist because of mode locking. Hot colors (reds) indicate either high period orbits or quasiperiodic trajectories. Below $k = 1$ quasiperiodic regions are interrupted by mode-locked regions which generally increase in width as $k$ increases. Evidence of period-doubling cascades can be seen above $k = 1$.

## 5. Definition of Sphere Map

The circle map is the composition of two simpler maps. The first is a rigid rotation of the circle through the angle $\omega_0$: $\theta \to \theta' = \theta + \omega_0$. This is a linear map. The second map is a nonlinear, sometimes noninvertible deformation of the circle: $\theta \to \theta' = \theta - k\sin(\theta)$. This nonlinear map involves a folding centered on the angle $\theta = 0$. It is noninvertible for $|k| > 1$.

We construct a nonlinear map of the sphere to itself by generalizing these two transformations. The linear step applies a rigid rotation of the sphere onto itself: $(X, Y, Z) \to (X, Y, Z)'$, where the sum of the squares of the coordinates is $+1$. It

consists of a rigid rotation through an angle $\omega$ about an axis of unit length $\mathbf{n}$: $\omega\mathbf{n} = (\omega_x, \omega_y, \omega_z)$.

The nonlinear step folds the sphere about the half of a great circle through the poles and the point $(1, 0, 0)$ ("Greenwich meridian"). The cut point for this map is the negative $X$ axis, so that the azimuthal angle $\phi$ satisfies $-\pi \leq \phi = \tan^{-1}(Y/X) \leq +\pi$. This angle is stretched according to $\phi \to \phi' = \phi - k\sin(\phi)$. The image coordinates on the sphere are $Z' = Z, X' = R\cos(\phi'), Y' = R\sin(\phi')$, where $R = \sqrt{X^2 + Y^2}$. This simple two-step map (rigid rotation + fold) is an extension of the circle map from $S^1$ to $S^2$. In this case the wrinkling exhibited in the circle map occurs as a folding centered on the half great circle described above.

The sphere map depends on $3 + 1$ parameters. Three identify an element in the rotation (Lie) group $SO(3)$, which acts through a linear representation on the coordinates $(X, Y, Z) \in S^2$. The fourth identifies the strength of a certain type of nonlinearity acting on the sphere surface $S^2$.

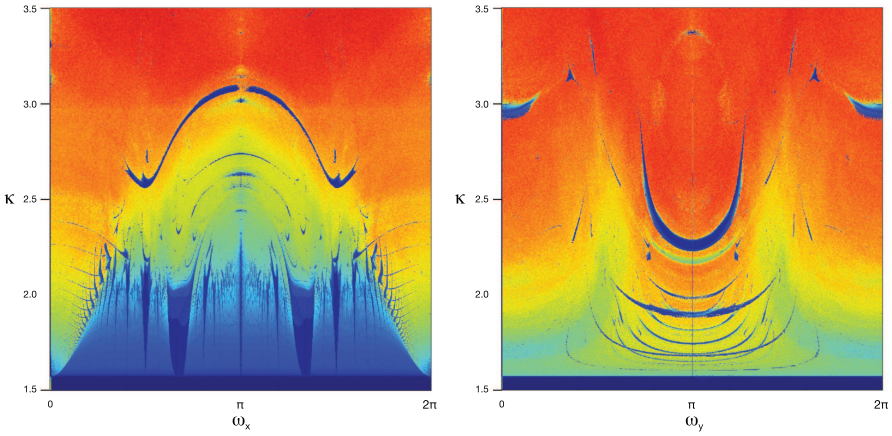


Fig. 2. (color online) Behavior of the sphere map for rotations about the: $x$-axis $(1, 0, 0)$ (left) and the $y$-axis $(0, 1, 0)$ (right). Color coding as in Fig. 1. Mode-locked regions can be seen somewhere for many values of $k$.

## 6. Scanning Procedure

To explore the sphere map we choose a rotation axis and describe the trajectories as the rotation angle $\omega$ and the nonlinear strength $k$ are varied. The trajectory is characterized by the value of the azimuthal angle $\phi$. For a period-$p$ orbit there will be $p$ distinct angular values. Each successive value of this angle is recorded in a trajectory and the angular values of these coordinates are binned. The number of

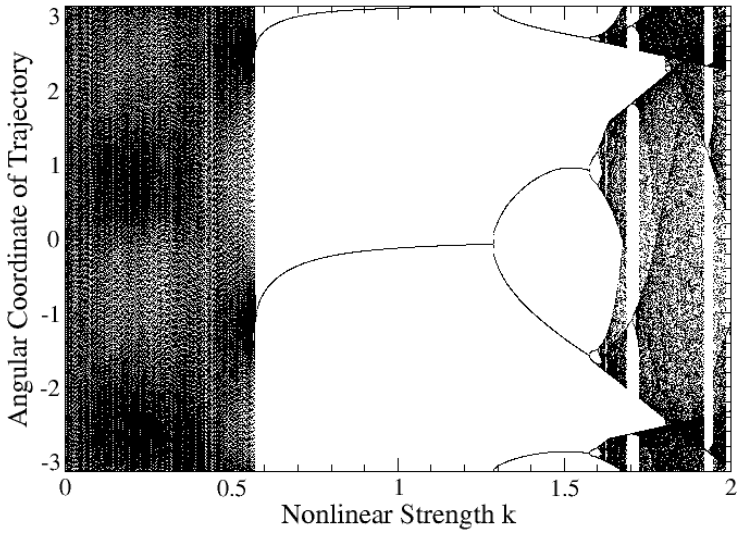


Fig. 3. Bifurcation diagram taken along $\omega = \pi \times 99/100$ in Fig. 1. Quasiperiodic behavior ($0 \leq k < 0.6$) is followed by mode locking ($0.57 \leq k \leq 1.3$), which is followed by period-doubling ($k \leq 1.3 \leq 1.6$) which is followed by chaotic behavior intermingled with periodic windows ($1.6 \leq k \leq 2.0$).

bins visited by a trajectory is determined and color coded in Figs. 1 and 2. Mode-locked orbits of period one and two are coded dark and light blue. Orbits of high period are generally indistinguishable from quasiperiodic orbits in this color plot. They can be distinguished by the structure of the bifurcation diagrams presented in Figs. 3-9. Further, chaotic behavior cannot occur unless the map is noninvertible, that is, for $|k| > 1$.

The results are shown in Fig. 1 for rotations around the $z$ axis $\mathbf{n} = (0, 0, 1)$. For $k < 1$ the motion is either quasiperiodic or mode-locked, with the mode-locked regions indicated by the dark blue color. These windows (tongues) generally increase in width with increasing $k$. Above $k = 1$ period doubling begins to occur (shades of lighter blue) leading to chaotic behavior. The chaotic regions are intermixed with mode locked regions, and the chaotic region has diminishing measure as $k$ continues to increase.

For rotations around the $x$- and $y$-axes the result is substantially different. In Fig. 2a we show the results for rotations around the $x$-axis. In this case mode-locking occurs for $k < 1.5$. As $k$ increases above 1.5 locking to higher period orbits occurs, leading eventually to quasiperiodic and chaotic behavior. Figure 2b shows a similar plot for rotations around the $y$-axis. Just as for rotations around the $x$-axis, mode-locking occurs for $k < 1.5$ and appears in isolated regions for larger values of $k$.

## 7. Bifurcation Cuts

We construct bifurcation diagrams for the results presented in Fig. 1 along various cuts. The first cut (Fig. 3), along $k$ in the range $0 \leq k \leq 2$, at constant rotation angle $\omega = \pi * (99/100)$, shows that the motion is quasiperiodic up to $k = 0.6$. After this point the invariant density increases to the point where a period-two orbit emerges. This continues until $k \simeq 1.3$ where a period-doubling cascade begins. The evolution along this cut terminates in a chaotic attractor for $k \simeq 1.6$. The chaotic regions show windows of mode locking intermingled with the chaotic behavior, typical of the logistic map. The largest window, at $k \simeq 1.7$, has period $2 \times 3$. It is the period-three window in the chaotic attractor based on the period-two orbit.

Figure 4 shows a cut at $k = 1$, below the range in which chaos is observed in Fig. 3. This figure shows in detail the behavior indicated in Fig. 1. There is an intermingling of mode-locked and quasiperiodic behavior as $\omega_z$ is scanned from $-\pi$ to $+\pi$. Mode locking to a period-one orbit occurs around $\omega_z = 0$. Mode locking to a period-two orbit occurs around $\omega_z = \pi = \frac{2\pi}{2}$. Mode locking to orbits of period $d = 3, 4, \ldots$ occurs around $\omega_z = \frac{2\pi}{d}$.

Another cut, at $k = 1.8$, is shown in Fig. 5. This figure only shows $0 \leq \omega_z \leq \pi$ because of two-fold rotational symmetry about the origin. As $\omega_z$ increases from 0 to $\pi$ mode locking is replaced by quasiperiodicity and then by mode-locking at

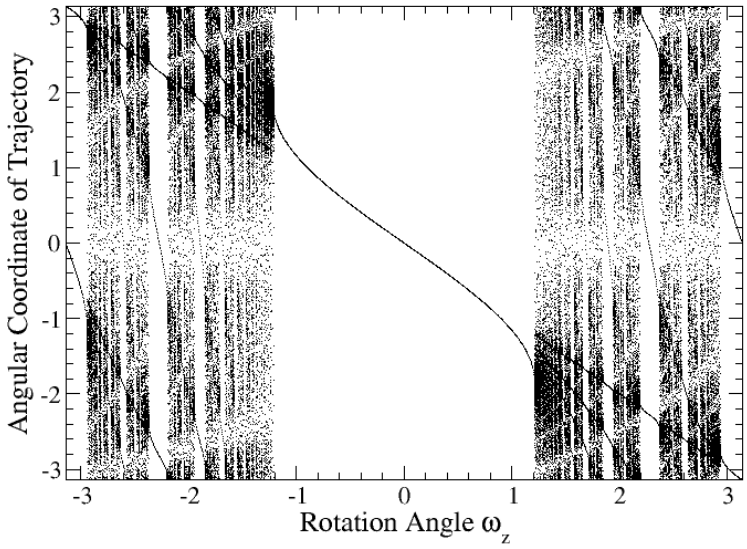


Fig. 4. Bifurcation diagram taken along $k = 1$ in Fig. 1. This bifurcation diagram shows intermingling of quasiperiodic behavior with mode locking. The largest mode-locked region occurs in the range $-1.2\pi < \omega_z < +1.2\pi$. Period-two mode locking occurs around $\pi$ radians, mode-locking of period three around $\pm\frac{2\pi}{3}$, period-four around $\pm\frac{2\pi}{4}$, etc.

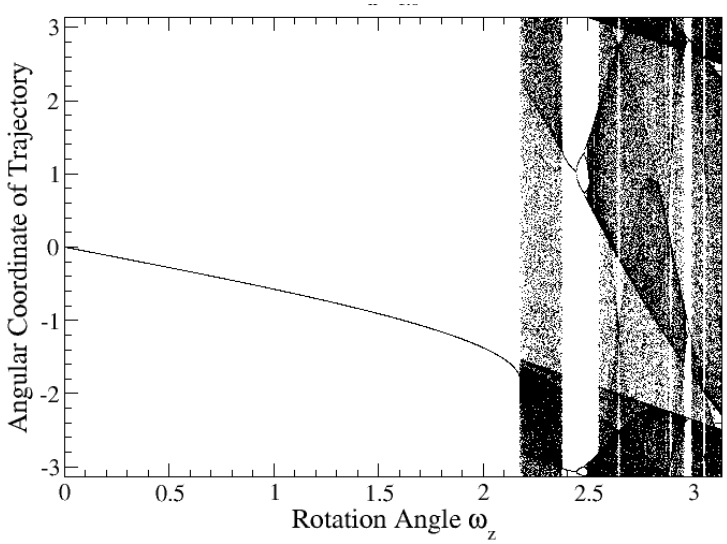


Fig. 5. Bifurcation diagram taken along $k = 1.8$ in Fig. 1 in the restricted range $0 \leq \omega_z \leq \pi$. This bifurcation diagram shows (left to right) how mode-locking gives way to quasiperiodicity which then gives way to period-doubling and then to chaos intermingled with periodic windows. This bifurcation diagram exhibits a two-fold rotational symmetry around the origin.

twice the period. A period-doubling cascade to chaos follows. As is typical, there are periodic windows in the chaotic region.

Figure 6 shows a bifurcation diagram for the scan in Fig. 2 at $k = 2.2$ as a function of the rotation angle $\omega_x$. Only the first half of this bifurcation diagram is shown since the diagram is symmetric under $\omega_x \to 2\pi - \omega_x$. The windows that appear in Fig. 6 generally undergo a period-doubling route to chaos. A region of period-doubling is magnified in Fig. 7.

A bifurcation diagram taken along the symmetry axis $\omega_y = \pi$ is shown in Fig. 8. A mode-locked period-one orbit undergoes period-doubling to chaos. At $k \simeq 2.85$, the chaotic attractor begins to wind around itself in the sense that its boundaries begin to overlap.

## 8. Trajectories

A trajectory consists of an iterated sequence of points $(X_i, Y_i, Z_i)$ on the sphere surface. The nonlinear transformation maps points from a given latitude ($Z$ value) to the same latitude, as do rigid rotations around the $Z$-axis. Composition of these two operations maps points into points with the same latitude. Projecting trajectories onto the equatorial plane maps them to a circle with fixed radius. As the strength of the nonlinearity $k$ is varied, the invariant density on this circle varies but its radius does not. These projections provide a simple visual method to classify

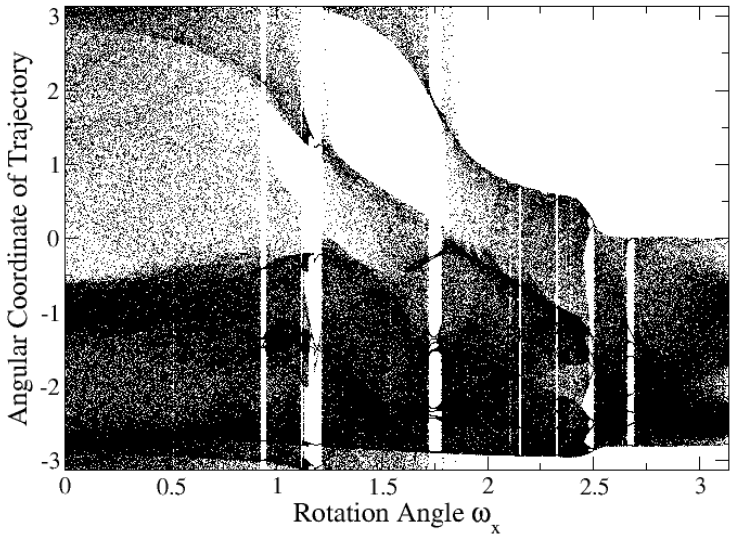


Fig. 6. A cut along $k = 2.2$ in Fig. 2 in the restricted range $0 \leq \omega_x \leq \pi$. This bifurcation diagram shows (left to right) how quasiperiodicity gives way to mode-locking and then to period-doubling to chaos.

trajectories. An ensemble of trajectories for $k$ values in the range $0.5 \leq k \leq 2.0$ is shown in Fig. 9. Since the latitude is invariant under these transformations all trajectories lie on the same circle. For visual clarity we scale the projection by a $k$-dependent factor $(1 + k)$. The resulting projections are organized into concentric rings. For small values of $k$ (interior region) quasiperiodic orbits predominate. For larger values of $k$ mode locking begins to occur. The first evident mode locking occurs for $p = 5$, followed by a period-doubling route to chaos. The next mode locking occurs for $p = 3$, again followed by a period-doubling cascade. The outside ring shows a period-two mode locking, also followed by a period-doubling route to chaos. For larger values of $k$ a period-one mode locking occurs. This behavior contrasts with the behavior of the circle map.

## 9. Summary and Discussion

Spin-torque oscillators are nanodevices with important technological promise. Isolated oscillators are described by the Landau-Lifshitz-Slonczewski equations. Since the magnitude of the magnetic moment is assumed constant within the LLS equations, the phase space for a spin valve is the surface of the sphere $S^2$. If a spin valve is periodically driven the phase space expands to $S^2 \times S^1$, so that chaotic behavior is possible. It is useful to study the dynamical properties of a periodically driven spin valve by investigating the first return map on a Poincaré surface of section — the sphere under stroboscopic measurements at $\phi = \text{cst.}$, $\phi \in S^1$.

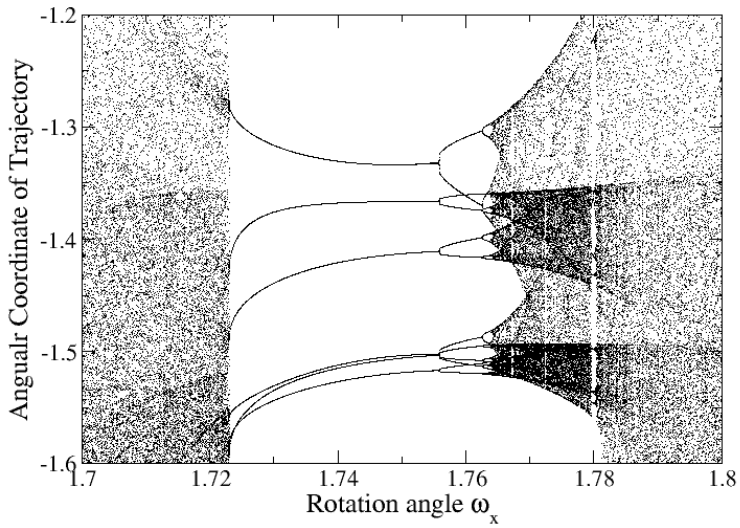


Fig. 7. This blow-up shows clearly how the mode-locked state goes through a period-doubling cascade to chaos, which then exhibits a crisis back to quasiperiodicity.

To accomplish this, we have generalized the circle map $S^1 \to S^1$ to a sphere map $S^2 \to S^2$. This sphere map is the composition of two maps. The first is a rigid rotation of the sphere to itself which is parametrized by three variables: the Euler angles or a rotation angle $\omega$ together with a rotation axis $\mathbf{n}$, or $(\omega_x, \omega_y, \omega_z)$. The second map is a deformation of the density on the sphere surface. We choose this nonlinear map as a fold around the Greenwich meridian, using exactly the same form as occurs in the circle map. The strength of this nonlinearity is defined by a parameter $k$.

Three scans have been made showing behavior in an $\omega - k$ plane. The first scan is for rigid rotations around the $z$ axis, and the results are similar to those encountered for the circle map. The other two scans involve rotations around the $x$- and $y$-axes. In these cases there is a mixture of quasiperiodicity, mode-locking, and chaos. However, the organization of these types of behavior is not yet well-understood.

Several bifurcation plots were made to better understand the information in the initial scans. The bifurcation plots show a systematic organization of the quasiperiodic, mode-locked, and chaotic regions.

Finally, we calculated trajectories under iterates of the sphere map. For rotations around the $z$ axis all iterates lie on a fixed latitude circle. These trajectories have been projected down to the equatorial plane and scaled by a $k$-dependent factor for visual clarity. These projections (c.f., Fig. 9) emphasize the intermingling of the quasiperiodic (dark) and mode-locked (mostly white) regions.

The sphere map depends on four parameters. Three identify an element in the

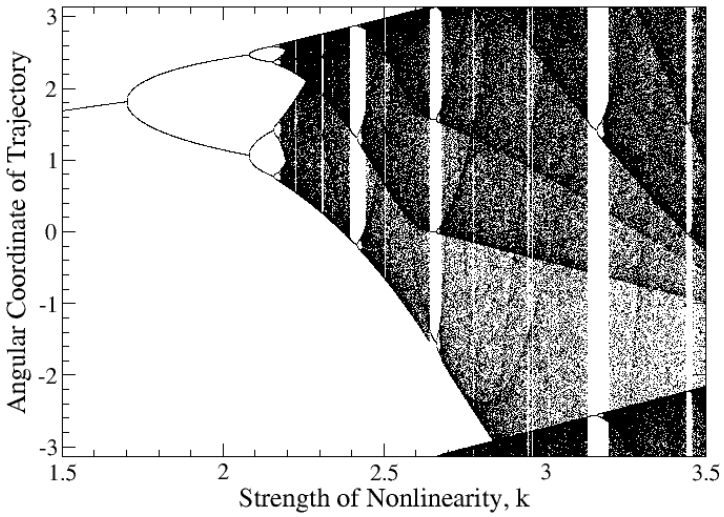


Fig. 8. Bifurcation diagram taken along the scan of Fig. 2 along the symmetry axis. This diagram exhibits the classic period-doubling scenario with a twist: the attractor begins to wind around itself for $k > 2.85$ when the boundaries of the basin of attraction begin to overlap.

rotation (Lie) group $SO(3)$. The fourth identifies the strength of a certain type of nonlinearity.

This paper developed out of a long series of discussions during which my father and I attempted to explain our research topics to one another. While we are both physicists, we pursue substantially different subtopics within physics. My father has constructed a career around non-linear dynamics and chaos theory while my initial research direction centered on magnetism in condensed matter systems. Fortunately, magnetic systems display a rich dynamic range, particularly because they can be driven both by magnetic fields and electric currents. This provided a natural opportunity for us to explore the possibility of chaotic dynamics in magnetic systems. We were pleasantly surprised by the wealth of behavior we found.

This work was supported in part by NSF Grant PHY 0754081.

## References

1. V. I. Arnold, Small denominators. I. On the mappings of the circumference onto itself, Trans. Am. Math. Soc. 2nd Ser. **46**, 213 (1965).
2. V. I. Arnold, Small denominators and problems of stability of motion in classical and celestial mechanics, Russian Math. Surveys **18**(6), 85-191 (1963).
3. E. A. Jackson, Perspectives on Nonlinear Dynamics, Cambrdige: University Press, 1989.
4. E. N. Lorenz, Deterministic nonperiodic flow, J. Atmos. Sci. **20**, 130-141 (1963), c.f., Eq. (4).

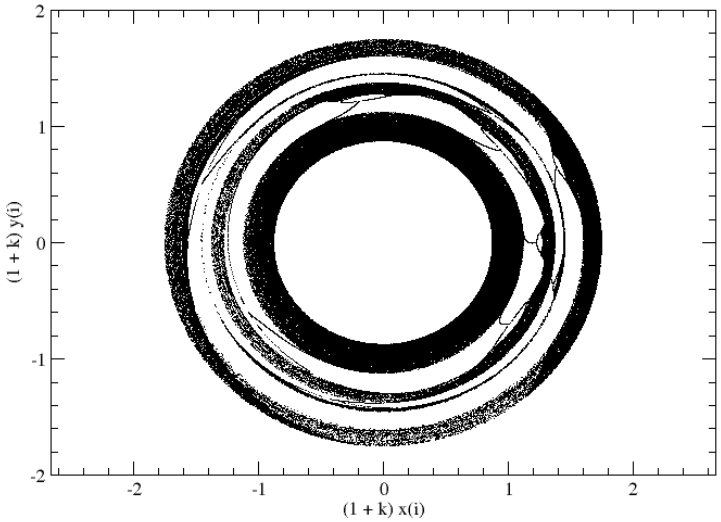


Fig. 9. Scaled projection of a trajectory for $0.5 \leq k \leq 2.0$. Trajectories are scaled by $(1 + k)$. Three rings of mode locked behavior are evident. These have period $p = 5, 3, 2$, respectively (from the inside). Each mode locking is followed by a period-doubling cascade to chaos.

5. H. D. I. Abarbanel, R. Brown, J. J. Sidorowich, and L. Sh. Tsimring, The analysis of observed chaotic data in physical systems, Revs. Mod. Phys. **64**(5), 1331-1393 (1993).
6. L.D. Landau and E.M. Lifshitz, Theory of the dispersion of magnetic permeability in ferromagnetic bodies, Phys. Z. Sowjetunion **8**, 153-169 (1935).
7. T.L. Gilbert, A Lagrangian formulation of the gyromagnetic equation of the magnetic field, Physical Review **100**, 1243 (1955).
8. T.L. Gilbert, Armor Foundation Research Project No. A059, Supplementary Report, May 1, 1956.
9. T.L. Gilbert, A phenomenological theory of damping in ferromagnetic materials, IEEE Trans. Mag. **40** (6), 3443-3449 (2004).
10. L. Berger, Low field magnetoresistance and domain drag in ferromagnets, J. Appl. Phys., **49**, 2156-2161 (1978).
11. L. Berger, J. Appl. Phys., **50**, 2137 (1979).
12. L. Berger, Emission of spin waves by a magnetic multilayer traversed by a current, Phys. Rev. B, **54**, 9353-9358 (1996).
13. J. C. Slonczewski, Current-driven excitation of magnetic multilayers, J. Magn. Magn. Mater., **159**, L1-L7 (1996).
14. J. Akerman, Science **308**, 508 (2005).
15. S. S. P. Parkin, M. Hayashi, and L. Thomas, Science **320**, 190 (2008).
16. W. H. Rippard, M. R. Pufall, S. Kaka, S. E. Russek, T. J. Silva, Phys. Rev. Lett., **92**, 027201, (2004).
17. O. Boulle, V. Cros, J. Grollier, L. G. Pereira, C. Deranlot, F. Petroff, G. Faini, J. Barnas, and A. Fert, Shaped angular dependence of the spin-transfer torque and microwave generation without magnetic field Nature Physics, **3**, 492-497 (2007).
18. P. M. Haney, R. A. Duine, A. S. Nunez, and A. H. MacDonald, J. Magn. Magn. Mater. **320**, 174412 (2008).

19. S. I. Kiselev, J. C. Sankey, I. N. Krivorotov, N. C. Emley, R. J. Schoelkopf, R. A. Buhrman, D. C. Ralph, Microwave oscillations of a nanomagnet driven by a spin-polarized current, Nature, **425**, 380383 (2003).
20. D. C. Ralph and M. D. Stiles, J. Magn. Magn. Mater. **320**, 1190 (2008).
21. R. Gilmore and M. Lefranc, *The Topology of Chaos*, NY: Wiley, 2002.
22. R. Gilmore and C. Letellier, *The Symmetry of Chaos*, Oxford: University Press, 2008.
23. Z. Li, Y. C. Li, and S. Chang, Dynamic magnetization states of a spin valve in the presence of dc and ac currents: Synchronization, modification, and chaos, Phys. Rev. B**74**, 954417 (2006).
24. Z. Yang, S. Zhang, and Y. C. Li, Chaotic dynamics of spin-valve oscillators, Phys. Rev. Lett. **99**, 134101 (2007).
25. M. Lakshmanan and K. Nakamura, Landau-Lifshitz equation of ferromagnetism: Exact treatment of the Gilbert damping, Phys. Rev. Lett. **53**, 2497-2499 (1984).
26. M. Lakshmanan, The fascinating world of the Landau-Lifshitz-Gilbert equation: An overview, Phil. Trans. Roy. Soc. A**369**, 1280-1300 (2011).